Journal of Manufacturing Engineering, March 2026, Vol. 21, Issue. 1, pp 025-035
DOI. https.//doi.org/10.37255/jme.v21i1pp025-035

INFLUENCE OF LATTICE INFILL GEOMETRY ON THE MECHANICAL RESPONSE OF FUSED FILAMENT FABRICATED ZIRCONIA FUNCTIONALLY GRADED STRUCTURES

Kathirvel V[1], Krishnaveni A[2], Jebakani D[3]

[1,2,3] Department of Mechanical Engineering, Government College of Engineering, Tirunelveli, Tamil Nadu, India

Abstract

Fused filament fabrication (FFF) enables the production of complex ceramic structures with tailored internal architecture. However, the influence of lattice infill geometry on the mechanical behaviour of zirconia-based functionally graded structures remains poorly characterised. This study systematically investigated the mechanical response and dimensional stability of zirconia functionally graded lattices incorporating grid, gyroid, and triangular infill patterns. Specimens were fabricated via extrusion-based FFF, followed by chemical debinding and high-temperature sintering. The mechanical performance was evaluated under compression, tension, and flexure in accordance with ASTM E9, E8, and C1161, respectively. Complementary porosity and shrinkage analyses were conducted to establish relationships between geometry and properties. Distinct topology-dependent mechanical behaviours were observed. The grid-based structures exhibited superior load-bearing capacity, sustaining maximum compressive loads of 26.0 ± 1.2 kN, followed by triangular (24.1 ± 1.5 kN) and gyroid (23.4 ± 1.8 kN) configurations. Under flexural loading, the grid lattices supported 20.0 ± 1.1 kN, compared to 15.8 ± 1.4 kN (triangular) and 11.0 ± 1.6 kN (gyroid). Tensile testing revealed similar trends: grid (15.0 ± 0.9 kN), triangle (11.5 ± 1.3 kN), and gyroid (9.7 ± 1.5 kN). Gyroid architectures demonstrated improved deformation tolerance despite lower peak loads. Shrinkage analysis confirmed geometry-dependent dimensional variations (19–22% linear shrinkage), consistent with the densification-driven behaviour typical of zirconia systems. These findings establish critical structure–property relationships for FFF-fabricated zirconia lattices, providing design guidance for lightweight ceramic components in mechanically demanding applications.

Keywords. *Fused filament fabrication, zirconia, functionally graded structures, lattice infill geometry, and mechanical behaviour.*

1. Introduction

Recent advances in additive manufacturing have fundamentally transformed the design and fabrication of architected materials, particularly lattice-structured systems engineered for tailored mechanical performance [1]. Unlike conventional manufacturing techniques, additive manufacturing enables precise control over internal geometries, allowing the creation of lightweight structures with enhanced stiffness-to-weight ratios, improved energy absorption, and tunable deformation behaviour [2][3]. This design flexibility has accelerated the adoption of lattice architectures across diverse engineering domains, including aerospace, automotive, energy, and biomedical applications [4] [5]. The ability to engineer internal topology without significant manufacturing constraints represents a paradigm shift in material design, where the mechanical response can be systematically controlled through structural geometry rather than solely through material composition [6]. Among the various additive manufacturing techniques, extrusion-based processes have attracted increasing attention owing to their versatility, scalability, and economic viability. These methods are compatible with a broad range of material systems, including polymers, composites, and advanced ceramics. Fused filament fabrication (FFF) has emerged as a practical and widely accessible extrusion-based technique capable of producing complex geometries with controlled porosity and structural gradients [7-10]. The layer-by-layer deposition mechanism inherent to FFF allows the fabrication of components with intricate lattice architectures that would be difficult or impossible to achieve using subtractive or formative processes [11-14]. While FFF has been extensively investigated for polymeric materials, its application to ceramic systems has opened

**Corresponding Author -E-mail. krishnaveni@gcetly.ac.in*

new opportunities for fabricating high-performance structures with functional and mechanical customizations [15]. Lattice architectures play a decisive role in determining the mechanical responses of additively manufactured components [16]. Previous studies have demonstrated that variations in unit-cell topology, strut arrangement, connectivity, and relative density strongly influence stiffness, strength, failure mechanisms, and energy dissipation behavior [17-20]. Periodic lattice geometries, characterized by repeating unit cells, provide predictable mechanical behaviour and ease of design optimization. Conversely, no periodic and stochastic architectures introduce additional complexity but may offer improved stress distribution and damage tolerance [21].

In recent years, triply periodic minimal surfaces (TPMSs) have gained prominence owing to their continuous surfaces, smooth curvature, and reduced stress concentration. Gyroid-based architectures, for instance, have been shown to exhibit favorable combinations of mechanical efficiency and permeability, making them attractive for multifunctional applications in soft robotics. Despite substantial progress in lattice structure research, the comparative influence of different lattice infill geometries within functionally graded ceramic systems remains insufficiently understood [22]. Much of the existing literature has focused on metallic and polymeric materials, where processing constraints, failure mechanisms, and deformation behaviours differ markedly from those observed in ceramics [23]. Ceramic materials exhibit distinct characteristics, including brittle fracture behaviour, high stiffness, and sensitivity to defects, which fundamentally alter the relationship between geometry and mechanical performance [24]. Consequently, insights derived from polymeric or metallic lattice studies cannot be directly generalized to ceramic lattice systems without careful experimental validation. Functionally graded structures have emerged as a powerful design strategy for improving structural efficiency and mechanical reliability [25]. Inspired by natural biological systems, functionally graded architectures introduce gradual spatial variations in density, porosity, and composition, enabling tailored property distributions within a single component. Such gradients reduce abrupt transitions in mechanical properties, mitigate stress concentrations, and enhance damage tolerance [26]. In biomedical engineering, graded structures are particularly relevant for bone scaffold applications, where mechanical stability must coexist with high porosity to facilitate tissue growth and nutrient transport. The hierarchical and graded nature of natural bone motivates the development of synthetic scaffolds that can mimic these structural characteristics [27]. Although functionally graded designs have been extensively explored in metals and polymers, investigations involving graded ceramic lattice structures remain comparatively limited. The fabrication of graded ceramics poses unique challenges in powder dispersion, binder removal, sintering kinetics, and dimensional stability. In extrusion-based additive manufacturing, these challenges are compounded by factors such as filament rheology, extrusion consistency, and interlayer bonding quality [28]. Consequently, the successful implementation of graded lattice designs in ceramic systems requires a comprehensive understanding of both the processing constraints and geometry-dependent behaviour. Ceramic biomaterials, particularly zirconia-based systems, have gained widespread recognition for their exceptional mechanical strength, fracture toughness, chemical stability, and biocompatibility properties. Zirconia exhibits transformation toughening mechanisms that enhance its crack resistance and mechanical reliability, distinguishing it from many other structural ceramics. These properties make zirconia highly attractive for load-bearing biomedical applications, including dental restorations, orthopedic implants, and bone substitutes. Furthermore, the favorable biological response and wear resistance characteristics of zirconia support its integration into advanced scaffold designs [29]. However, the additive manufacturing of zirconia components remains challenging owing to issues such as binder elimination, defect formation, and sintering-induced shrinkage. Dimensional variations during sintering are a critical concern in ceramic additive manufacturing. Shrinkage behaviour is influenced by multiple factors, including particle packing density, thermal gradients, and geometric constraints imposed by the lattice architectures [30].

In lattice-structured components, non-uniform densification may lead to distortion, residual stresses, or microstructural discontinuities [31]. These effects directly affect mechanical performance, underscoring the need to evaluate geometry-dependent shrinkage behaviour alongside conventional mechanical characterization. Additionally, microstructural features such as interlayer boundaries, porosity distribution, and localized defects significantly influence the failure mechanisms of additively manufactured ceramics [32]. Although FFF has been widely adopted for polymeric systems, its application to zirconia-based lattice structures introduces additional considerations related to extrusion stability, filament composition, densification behaviour, and microstructural integrity [33]. In particular, the lattice infill geometry may critically affect the load transfer pathways, stress distribution, porosity characteristics, and dimensional stability during post-processing [34]. Therefore, a systematic investigation of these relationships is essential for the reliable design and optimization of ceramic lattice components intended for mechanically demanding applications [35]. The present study investigates the influence of lattice infill geometry on the mechanical

Journal of Manufacturing Engineering, March 2026, Vol. 21, Issue. 1, pp 025-035
DOI. https.//doi.org/10.37255/jme.v21i1pp025-035

response of functionally graded zirconia structures fabricated via FFF. Distinct lattice configurations, including grid, gyroid, and triangular patterns, were examined to evaluate their effects on mechanical behaviour, porosity, and dimensional stability. By integrating functionally graded design principles with extrusion-based ceramic additive manufacturing, this study aims to clarify the structure–property relationships governing zirconia lattice systems and provide guidance for architectural selection. The novelty of this research lies in the comparative assessment of lattice infill geometries within zirconia functionally graded structures fabricated via fused filament fabrication. Unlike prior investigations that predominantly focused on metallic or polymeric materials, this study addresses ceramic-specific processing effects, including debinding and sintering-induced dimensional variations, as well as geometry-dependent mechanical behaviour. These findings contribute to a deeper understanding of the processing–structure–property interactions in ceramic additive manufacturing and support the development of mechanically reliable zirconia lattice structures for advanced engineering and biomedical applications.

2. Materials and methods

2.1. Material System

All specimens were fabricated using a commercially available zirconia-based ceramic filament (Zetamix Black Zirconia; Nanoe SA, France). The filament comprised 3 mol% yttria-stabilised zirconia (3Y-TZP) particles (average particle size: ~40 nm) dispersed within a thermoplastic binder matrix designed for extrusion-based additive manufacturing. According to the manufacturer's technical datasheet, the filament contains approximately 85-87 vol. % ceramic loading, ensuring structural integrity during printing and enabling effective densification after sintering. Zirconia (3Y-TZP) was selected for its superior mechanical strength (flexural strength>800 MPa), fracture toughness (>5 MPa•$m^{1/2}$), chemical stability, and established relevance for load-bearing biomedical applications. Prior to fabrication, the filament was inspected for dimensional consistency (diameter: 1.75 ± 0.05 mm) to minimize the potential for extrusion irregularities.

2.2. Design of functionally graded lattice structures

Functionally graded lattice specimens were designed using computer-aided design (CAD) software (SolidWorks 2021; Dassault Systèmes). All samples were designed with identical external dimensions in accordance with the respective ASTM standards, whereas the internal lattice topology and density distribution were systematically varied. Functional grading was achieved through a controlled linear variation in lattice density (60% to 80% infill density), enabling gradual porosity transitions along the specimen length. Three lattice infill geometries were investigated: grid (orthogonal), gyroid (triply periodic minimal surface), and triangular. These architectures were selected to represent structurally distinct load-transfer mechanisms: axially dominated (grid), shear-assisted (triangular), and curvature-mediated (gyroid) deformation behaviours. Representative CAD models are shown in Fig. 1.

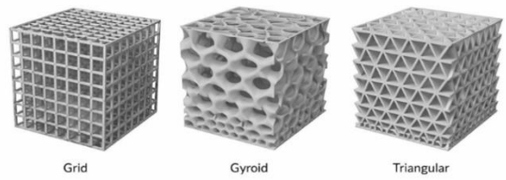

Fig. 1. Representative CAD models of lattice infill geometries used for the specimen design, illustrating the grid, gyroid, and triangular architectures with graded density distributions.

2.3. Additive manufacturing via fused filament fabrication

The lattice structures were fabricated using an extrusion-based fused filament fabrication (FFF) system (Zetamix Printer, Nanoe SA). The printing parameters were selected based on validated processing conditions for zirconia-filled filaments and optimised through preliminary trials. A nozzle temperature of 180 ± 2 °C was employed to ensure adequate softening of the binder phase and the stable extrusion of the filament. The build plate temperature was maintained at 40 ± 2 °C to enhance the interlayer adhesion during deposition. A nozzle diameter of 0.6 mm was selected to improve extrusion stability and reduce the risk of clogging commonly associated with ceramic-filled feedstocks. Layer height was fixed at 0.2 mm, balancing geometric resolution and deposition consistency. The printing speed was maintained at 25 mm•s^{-1} to ensure continuous filament flow without inducing excessive shear stresses or extrusion defects. All specimens were produced using a vertical build orientation (z-axis) to maintain structural uniformity and minimise geometric distortion. Five replicates (n=5) were fabricated for each lattice geometry and test condition to ensure statistical reliability. The fabrication parameters are listed in Table 1.

2.4. Debinding procedure

Following fabrication, the printed green bodies underwent a two-stage debinding process to remove the thermoplastic binder. Initial binder extraction was

Journal of Manufacturing Engineering, March 2026, Vol. 21, Issue. 1, pp 025-035
DOI. https.//doi.org/10.37255/jme.v21i1pp025-035

performed via solvent debinding in an acetone bath (99.5% purity) maintained at 40 ± 1 °C for 4 h, removing soluble binder constituents while preserving structural integrity. After solvent treatment, the specimens were dried under ambient conditions (23 ± 2 °C, 45% relative humidity) for 24 h to eliminate residual solvent. Thermal debinding was subsequently conducted in a programmable muffle furnace (Nabertherm GmbH, Germany) using a controlled heating schedule. A slow heating rate of 8 °C·h⁻¹ was applied from room temperature to 500 °C, with a 2 h dwell at 500 °C to ensure the complete decomposition of the remaining binder components while minimising the internal stresses that could lead to crack formation or distortion.

2.5. Sintering cycle

Densification of the debound specimens was achieved via high-temperature sintering in ambient air. The sintering cycle involved heating from room temperature to 1475 °C at a controlled rate of 50 °C·h⁻¹, followed by a 2 h holding period at the peak temperature to ensure complete consolidation of zirconia particles. Controlled cooling at 100 °C·h⁻¹ was applied to 500 °C, followed by natural furnace cooling to reduce the residual thermal stresses. The sintering process resulted in isotropic linear shrinkage of 21.5 ± 1.2% (determined from preliminary measurements), consistent with the manufacturer's specifications and the typical densification behaviour of zirconia-based ceramics.

2.6. Mechanical characterization

The mechanical performance of the sintered lattice specimens was evaluated using a universal testing machine (Instron 5969, 50 kN load cell) under displacement-controlled loading conditions (crosshead speed: 0.5 mm·min⁻¹). All tests were conducted at an ambient temperature (23 ± 2 °C). Five replicates (n=5) were tested for each test type and lattice geometry. Compression testing was conducted in accordance with the ASTM E9 standard using cubic specimens (nominal sintered dimensions: 17 × 17 × 16 mm³). Tensile testing was performed following the ASTM E8 standard using dog-bone specimens (nominal sintered gauge dimensions: 40 × 10 × 4 mm³). Flexural strength measurements were performed in three-point bending according to ASTM C1161, using bar specimens (nominal sintered dimensions: 60 × 10 × 4 mm³) with a support span of 40 mm. The ultimate load (N), ultimate stress (MPa), and strain-to-failure (%) were recorded for each specimen. The load-displacement data were acquired at a sampling frequency of 10 Hz.

2.7. Dimensional and shrinkage analysis

Dimensional stability was assessed by measuring the specimen geometry at three critical stages: after printing (green state), after debinding (brown state), and after sintering (final state). Measurements were performed using digital calipers (Mitutoyo, accuracy ±0.01 mm) at five marked locations per dimension. Linear shrinkage (%) was calculated using Equation (1).

$$Shrinkage\ (\%) = \left[\frac{(D_{green} - D_{sintered})}{D_{green}}\right] \times 100 \qquad (1)$$

where Dgreen and Dsintered represent the dimensions in the green and sintered states, respectively. Volumetric shrinkage was calculated from the dimensional measurements.

2.8. Microstructural characterization

The selected fractured specimens were examined using scanning electron microscopy (SEM, JEOL JSM-IT500) to assess the interlayer integrity, pore morphology, and fracture characteristics. The samples were sputter-coated with gold prior to imaging to prevent charging. Secondary electron images were acquired at accelerating voltages of 5-10 kV.

2.9. Statistical analysis

All quantitative data are presented as mean ± standard deviation (SD) based on five replicates (n=5). Statistical comparisons between the lattice geometries were performed using one-way analysis of variance (ANOVA), followed by Tukey's post hoc test, with a significance level of $p < 0.05$. All statistical analyses were conducted using the OriginPro 2021 software.

Table 1. Fused filament fabrication parameters used for the zirconia lattice specimen production.

Parameter	Value
Nozzle temperature	180 ± 2 °C
Build plate temperature	40 ± 2 °C
Nozzle diameter	0.6 mm
Layer height	0.2 mm
Printing speed	25 mm·s⁻¹
Build orientation	Vertical (z-axis)
Infill density range	60-80% (graded)
Infill geometries	Grid / Gyroid / Triangular
Number of replicates per condition	5

Journal of Manufacturing Engineering, March 2026, Vol. 21, Issue. 1, pp 025-035
DOI. https.//doi.org/10.37255/jme.v21i1pp025-035

3. Results

3.1. Dimensional accuracy and shrinkage behavior

The dimensional evolution of the zirconia lattice specimens during processing revealed consistent shrinkage behaviour, with geometry-dependent variations. Table 2 summarises the dimensional changes from the green (as-printed) to sintered states for all lattice configurations. The overall linear shrinkage ranged from 19.0% to 21.2% across all geometries, consistent with the expected isotropic shrinkage of 21.5 ± 1.2% reported by the filament manufacturer. Grid structures exhibited the most uniform shrinkage (coefficient of variation: 5.2%), whereas gyroid geometries showed slightly higher anisotropy, particularly in the width direction (gyroid compression specimens: 18.0 ± 0.5 mm vs. 17.0 ± 0.3 mm in length), suggesting curvature-induced densification gradients.

Table 2. Dimensional changes of zirconia lattice specimens through processing stages (mean ± SD, n=5).

Test Type	Geometry	Stage	Length (mm)	Width (mm)	Height (mm)	Linear Shrinkage (%)
Compression (nominal: 20×20×20 mm³)	Grid	Green	20.0 ± 0.2	20.0 ± 0.2	20.0 ± 0.2	—
		Sintered	17.0 ± 0.3	17.0 ± 0.3	15.0 ± 0.3	20.5 ± 1.1
	Triangular	Green	21.0 ± 0.2	21.0 ± 0.2	20.0 ± 0.2	—
		Sintered	17.0 ± 0.4	17.0 ± 0.4	16.0 ± 0.3	21.2 ± 1.3
	Gyroid	Green	21.0 ± 0.2	21.0 ± 0.2	20.0 ± 0.2	—
		Sintered	17.0 ± 0.4	18.0 ± 0.5	16.0 ± 0.4	20.8 ± 1.4
Flexural (70×10×5 mm³)	Grid	Green	75.0 ± 0.3	14.5 ± 0.2	5.0 ± 0.1	—
		Sintered	60.0 ± 0.5	10.0 ± 0.3	3.5 ± 0.2	21.0 ± 1.2
	Triangular	Green	74.0 ± 0.3	14.5 ± 0.2	4.0 ± 0.1	—
		Sintered	60.0 ± 0.5	12.0 ± 0.4	4.0 ± 0.2	19.8 ± 1.3
	Gyroid	Green	74.0 ± 0.3	14.0 ± 0.2	5.0 ± 0.1	—
		Sintered	60.0 ± 0.6	11.0 ± 0.4	4.0 ± 0.2	20.5 ± 1.4
Tensile (100×10×6 mm³)	Grid	Green	104.0 ± 0.4	14.5 ± 0.2	6.0 ± 0.1	—
		Sintered	102.0 ± 0.6	13.0 ± 0.3	4.4 ± 0.2	19.5 ± 1.0
	Triangular	Green	105.0 ± 0.4	14.0 ± 0.2	5.0 ± 0.1	—
		Sintered	100.0 ± 0.7	13.5 ± 0.4	4.4 ± 0.2	20.2 ± 1.2
	Gyroid	Green	104.0 ± 0.4	14.0 ± 0.2	5.0 ± 0.1	—
		Sintered	103.0 ± 0.8	13.5 ± 0.4	6.0 ± 0.3	19.0 ± 1.3

3.2. Compressive behavior

Compressive testing revealed a distinct geometry-dependent mechanical response. Figure 2a shows the representative load-displacement curves for each lattice configuration, while Table 3 summarizes the compressive properties. The grid lattice structures sustained the highest compressive loads (26.0 ± 1.2 kN), significantly exceeding those of the triangular (24.1 ± 1.5 kN, $p < 0.05$) and gyroid (23.4 ± 1.8 kN, $p < 0.01$) configurations. The ultimate compressive stress followed the same trend: grid (90.5 ± 4.2 MPa), triangular (83.8 ± 5.1 MPa), and gyroid (81.3 ± 6.2 MPa) patterns. The strain at failure exhibited an inverse relationship with strength. Gyroid specimens exhibited the highest deformation capacity (5.8 ± 0.5%), followed by triangular (5.1 ± 0.4%) and grid (4.2 ± 0.3%) geometries ($p < 0.05$ for all pairwise comparisons). This indicates a trade-off between the load-bearing capacity and deformation tolerance.

3.3. Tensile behavior

Tensile testing revealed more pronounced geometry-dependent differences than compression testing, reflecting the sensitivity of brittle ceramics to tensile stress concentrations. Table 4 presents the tensile properties of the composites. Grid structures demonstrated superior tensile load capacity (15.0 ± 0.9 kN), approximately 30% higher than triangular (11.5 ± 1.3 kN, $p < 0.001$) and 55% higher than gyroid (9.7 ± 1.5 kN, $p < 0.001$) configurations, respectively. The ultimate tensile stress followed an identical ranking. The failure strains remained low across all geometries (<1.5%), consistent with brittle ceramic behaviour. Gyroid specimens exhibited slightly higher tensile strain (1.3 ± 0.2%) compared to grid (0.9 ± 0.1%) and triangular (1.1 ± 0.2%) geometries ($p < 0.05$). Figure 3a shows representative tensile load-displacement curves,

Journal of Manufacturing Engineering, March 2026, Vol. 21, Issue. 1, pp 025-035
DOI. https://doi.org/10.37255/jme.v21i1pp025-035

revealing an abrupt failure in the grid structures versus a more gradual load drop in the gyroid specimens. Fracture surfaces (Figure 3b) confirmed interlayer delamination as the dominant failure mode, which was particularly evident in the triangular and gyroid configurations.

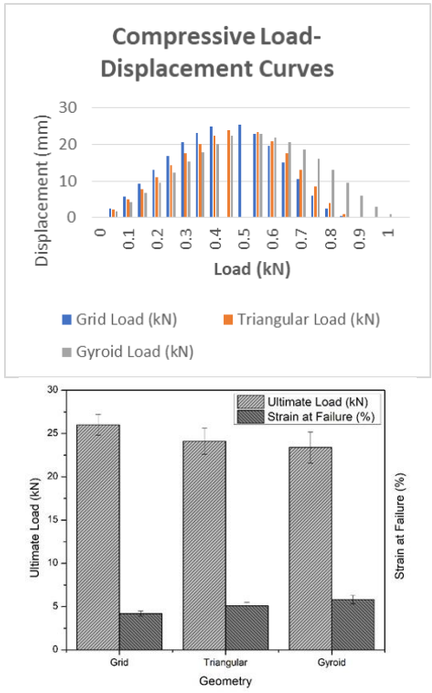

Fig. 2. (a) Compressive load-displacement curves for the lattice geometries. (b) Comparison of ultimate load and failure strain.

3.4. Flexural behavior

Three-point bending tests further confirmed the topology-dependent mechanical properties. Table 5 summarises the flexural properties. The grid lattice specimens sustained the highest flexural loads (20.0 ± 1.1 kN), significantly exceeding those of the triangular (15.8 ± 1.4 kN, $p < 0.001$) and gyroid (11.0 ± 1.6 kN, $p < 0.001$) specimens. The flexural strength followed the same trend: grid (42.7 ± 2.3 MPa), triangular (33.7 ± 3.0 MPa), and gyroid (23.5 ± 3.4 MPa). As observed in compression and tension, the failure strain increased with decreasing strength. Gyroid specimens exhibited the highest flexural strain (1.8 ± 0.3%), followed by triangular (1.5 ± 0.3%) and grid (1.2 ± 0.2%) geometries ($p < 0.05$). Figure 4 presents representative flexural load-displacement curves, illustrating the progressive failure in gyroid structures compared to the catastrophic failure in grid specimens. Crack initiation consistently occurred on the tensile surface of the bent specimens, confirming a tension-dominated failure.

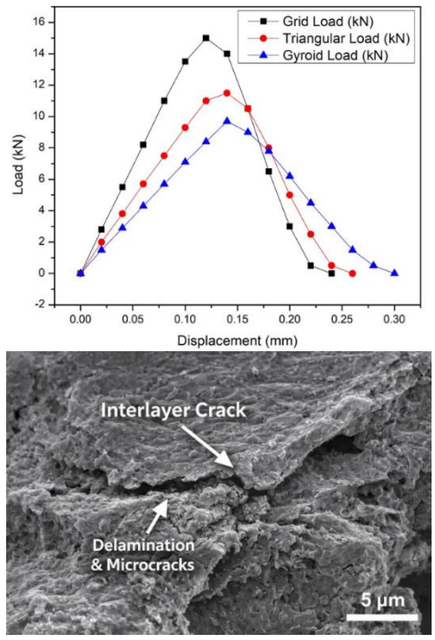

Fig. 3. (a) Representative tensile load-displacement curves for the zirconia lattice specimens. (b) SEM micrographs of the fracture surfaces showing interlayer failure.

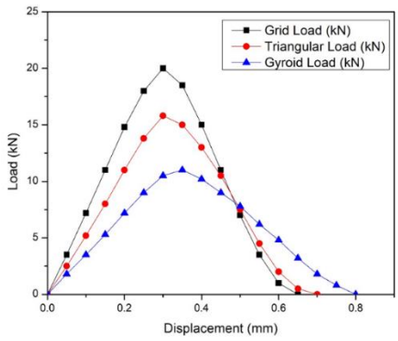

Fig. 4. Representative flexural load-displacement curves for the zirconia lattice specimens under three-point bending.

3.5. Porosity and microstructural features

SEM examination revealed the microstructural characteristics intrinsic to FFF-fabricated zirconia. Figure 5 shows representative micrographs of the sintered specimens. Interlayer boundaries were clearly identifiable (Figure 5) and exhibited a higher defect density than the strut interiors. Residual porosity was observed at two scales: (i) interlayer voids (~10-30 µm) resulting from incomplete filament fusion and (ii) intrastrut micropores (~1-5 µm) attributable to binder burnout and sintering

Journal of Manufacturing Engineering, March 2026, Vol. 21, Issue. 1, pp 025-035
DOI. https.//doi.org/10.37255/jme.v21i1pp025-035

kinetics. The grid structures demonstrated improved interlayer fusion (Figure 5), with fewer and smaller interlayer voids than the triangular and gyroid geometries. Gyroid specimens exhibited curvature-associated voids in regions of high geometric curvature, suggesting that complex surfaces impede uniform particle packing during deposition.

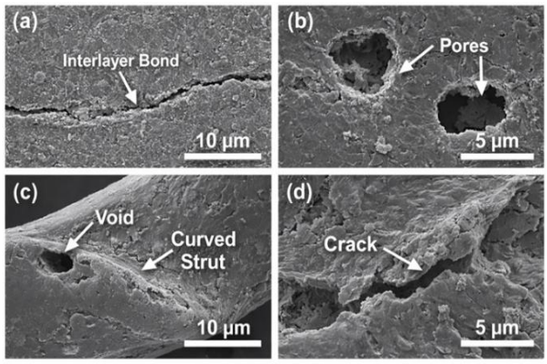

Fig. 5. SEM micrographs of sintered zirconia lattice specimensTable 3. Compressive properties of zirconia lattice specimens (mean ± SD, n=5).

Geometry	Ultimate Load (kN)	Ultimate Stress (MPa)	Strain at Failure (%)
Grid	26.0 ± 1.2	90.5 ± 4.2	4.2 ± 0.3
Triangular	24.1 ± 1.5	83.8 ± 5.1	5.1 ± 0.4
Gyroid	23.4 ± 1.8	81.3 ± 6.2	5.8 ± 0.5

Table 4. Tensile properties of the zirconia lattice specimens (mean ± SD, n=5).

Geometry	Ultimate Load (kN)	Ultimate Stress (MPa)	Strain at Failure (%)
Grid	15.0 ± 0.9	28.8 ± 1.7	0.9 ± 0.1
Triangular	11.5 ± 1.3	22.1 ± 2.5	1.1 ± 0.2
Gyroid	9.7 ± 1.5	18.6 ± 2.9	1.3 ± 0.2

Table 5. Flexural properties of zirconia lattice specimens (mean ± SD, n=5).

Geometry	Ultimate Load (kN)	Flexural Strength (MPa)	Strain at Failure (%)
Grid	20.0 ± 1.1	42.7 ± 2.3	1.2 ± 0.2
Triangular	15.8 ± 1.4	33.7 ± 3.0	1.5 ± 0.3
Gyroid	11.0 ± 1.6	23.5 ± 3.4	1.8 ± 0.3

4. Discussion

4.1 Topology-dependent deformation mechanisms

The experimental results demonstrate that the lattice infill geometry fundamentally governs the mechanical response of FFF-fabricated zirconia structures. The consistent mechanical hierarchy (grid > triangular > gyroid) across compression, tension, and flexure indicates that topology-controlled stress redistribution, rather than material variability, dominates the structural behaviour of these ceramic lattices. The grid architectures exhibited superior load-bearing capacity across all loading modes owing to their dominance in axial load transfer. Under compression, vertically aligned struts primarily experience axial stresses, which represent the most favourable stress state for brittle ceramics [1]. Axial compression suppressed crack opening and delayed catastrophic fracture initiation, explaining the 8-11% higher compressive strength of the grid structures compared to the triangular and gyroid geometries. This observation aligns with cellular solid theory, in which structures with axially loaded members exhibit stiffness scaling linearly with relative density, whereas bending-dominated structures exhibit quadratic or cubic scaling [2].

Triangular lattices demonstrated intermediate mechanical performance, reflecting their mixed deformation modes. Inclined struts redistribute the applied loads through combined axial and bending stresses, generating localised tensile stress concentrations at the strut junctions, even under global compression [3]. In flaw-sensitive zirconia, these tensile regions serve as preferential sites for crack initiation, thereby reducing the peak load capacity. However, the progressive failure observed in the triangular specimens (as evident in the load-displacement curves) suggests that inclined networks facilitate gradual load redistribution, potentially improving energy absorption before catastrophic failure. Gyroid structures, despite exhibiting the lowest peak strength, demonstrated superior deformation tolerance across all loading modes (23-50% higher failure strain than grid geometries). This behaviour arises from the curvature-mediated stress dispersion characteristic of triply periodic minimal surface architectures [4]. Continuous curved surfaces eliminate sharp junctions, thereby reducing stress concentration factors and distributing loads over larger volumes. However, the absence of dominant axial load paths results in bending-dominated deformation, reducing the stiffness and peak strength. Similar trade-offs between strength and ductility have been reported in polymer and metallic TPMS structures [5,6], but the present study confirms that this behaviour extends to brittle ceramic systems.

Journal of Manufacturing Engineering, March 2026, Vol. 21, Issue. 1, pp 025-035
DOI. https.//doi.org/10.37255/jme.v21i1pp025-035

4.2. Structure-property relationships in zirconia lattices

The observed mechanical hierarchy cannot be explained solely by the relative density, as all specimens were designed with comparable graded infill strategies (60-80%). However, the results revealed that topology-controlled stress distribution and defect sensitivity govern the mechanical performance of ceramic lattices. The relationship between the lattice geometry and mechanical response can be understood using two complementary frameworks. First, from a mechanics perspective, the stiffness and strength of lattice structures scale with the proportion of axially loaded members [7]. Grid geometries maximise this proportion, triangular geometries provide intermediate values, and gyroid geometries minimise the axial load paths. This explains the consistent ranking across the loading modes. Second, from a defect sensitivity perspective, bending-dominated geometries amplify the mechanical effects of processing-induced flaws. FFF-fabricated zirconia inherently contains microstructural discontinuities, including interlayer boundaries (Figure 5a) and residual pores. [8]. Under bending-dominated deformation, these defects experience amplified local stresses, thereby accelerating crack initiation. This mechanism explains why the strength difference between the grid and gyroid structures was most pronounced under flexural loading (82% higher for the grid) than under compression (11% higher). Flexural loading generates tensile stresses on the specimen surfaces, where interlayer defects are most prevalent. The strain-to-failure data provide additional insights into topology-dependent damage tolerance. Gyroid specimens consistently exhibited higher failure strains (4.2-5.8% compression, 1.3% tension, 1.8% flexure) than grid structures (4.2% compression, 0.9% tension, 1.2% flexure). This inverse strength-ductility relationship suggests that architectures promoting distributed stress fields delay localised failure, enabling more extensive microcracking before catastrophic fracture [9]. For applications requiring damage tolerance (e.g., impact-resistant components), gyroid geometries may offer advantages despite their lower peak strength.

4.3 Influence of processing on structure-property relationships

Microstructural observations (Section 3.5) confirmed that FFF-specific defects interact strongly with the lattice geometry to determine the mechanical performance. Interlayer boundaries represent mechanically vulnerable regions where incomplete diffusion bonding during sintering limits the load transfer between deposited layers [10]. Under tensile or flexural loading, these interfaces experience direct opening stresses, which explains their significantly lower tensile strengths (15-28 MPa) compared to compressive strengths (81-90 MPa). Geometry-dependent variations in the shrinkage behaviour (Table 2) further demonstrate the processing-structure interactions. Gyroid specimens exhibited slight anisotropic shrinkage, particularly in the curved regions, suggesting that the complex surface curvature introduces densification gradients [11]. During sintering, the differential densification rates between the curved and straight regions generate residual stresses that may persist in the final components. These stresses could contribute to the reduced load capacity of gyroid structures, particularly under tensile loading, where residual tensile stresses would exacerbate flaw sensitivity. The improved interlayer fusion observed in the grid structures (Figure 5b) may reflect a more favourable deposition geometry. Orthogonal strut networks provide continuous support to subsequent layers, promoting uniform compaction and interlayer contact. In contrast, the inclined and curved geometries characteristic of triangular and gyroid architectures introduce overhanging regions where the layer support is reduced, potentially compromising interlayer bonding [12].

4.4. Comparison with Literature

The mechanical properties obtained in this study align with the reported values for additively manufactured zirconia, although variations in testing standards and specimen geometries complicate direct comparison. For FFF-fabricated zirconia, previous studies have reported flexural strengths of 30-50 MPa for simple bar geometries [13,14], comparable to the 23-43 MPa range observed for lattice structures in the present work. The reduced strength of the lattice specimens relative to the theoretical values for dense zirconia (>800 MPa) reflects both the intentionally porous architecture and the processing-induced defects. Compared to polymer-based lattice studies, the strength hierarchy observed here (grid > triangular > gyroid) differs from some reports in which TPMS structures outperform truss-based geometries [15]. This discrepancy highlights the material-specific nature of topology optimisation; conclusions drawn from ductile polymers or metal lattices do not directly translate to brittle ceramic systems. In polymers, local yielding at stress concentrations redistributes loads and mitigates failure [16]; in ceramics, identical stress concentrations initiate catastrophic fractures.

5. Conclusions

This study systematically investigated the influence of lattice infill geometry on the mechanical response and dimensional stability of functionally graded zirconia structures fabricated via FFF. Based on a comprehensive experimental evaluation of grid, triangular,

and gyroid architectures under compression, tension, and flexural loading, the following conclusions can be drawn:

i. The lattice infill geometry fundamentally governs the mechanical behaviour of FFF-fabricated zirconia structures. Despite the identical material composition and processing conditions, distinct topology-dependent mechanical responses were observed across all loading modes, confirming that architectural design dominates the structural performance of ceramic lattice systems.
ii. Grid architectures provided superior load-bearing capacity, sustaining the highest compressive (26.0 ± 1.2 kN), flexural (20.0 ± 1.1 kN), and tensile (15.0 ± 0.9 kN) loads. This enhanced performance is attributed to the dominance of axial load transfer, which minimises bending-induced tensile stresses in this flaw-sensitive ceramic material.
iii. Triangular geometries exhibited balanced mechanical behaviour, with intermediate strength (compressive: 24.1 ± 1.5 kN; flexural: 15.8 ± 1.4 kN; tensile: 11.5 ± 1.3 kN) and progressive failure characteristics. Inclined strut networks facilitate mixed deformation modes, enabling gradual load redistribution before catastrophic fracture.
iv. Gyroid architectures exhibit superior deformation tolerance despite reduced peak strength. Gyroid specimens demonstrated 23-50% higher failure strains across all loading modes compared to grid geometries, attributable to curvature-mediated stress dispersion. This strength-ductility trade-off offers design opportunities for applications that require damage tolerance.
v. The shrinkage behaviour exhibited geometry-dependent variations, with an overall linear shrinkage ranging from 19.0% to 21.2% across all configurations. The grid structures exhibited the most uniform densification, whereas the gyroid geometries displayed slight anisotropy, suggesting that the complex surface curvature influences the sintering kinetics.
vi. Interlayer integrity governs failure initiation in FFF-fabricated zirconia lattice structures. SEM analysis confirmed that the interlayer boundaries represent mechanically vulnerable regions, with defect sensitivity amplified in bending-dominated architectures. The grid structures demonstrated improved interlayer fusion, contributing to their superior mechanical performance.
vii. The structure-property relationships in ceramic lattices are material-specific. The observed mechanical hierarchy (grid > triangular > gyroid) differs from that observed in some polymer-based lattice studies, confirming that design principles derived from ductile materials cannot be directly translated to brittle ceramic systems without experimental validation.
a. Functionally graded design strategies (60-80% density variation) successfully enabled property gradients while maintaining structural integrity, demonstrating the feasibility of fabricating zirconia components with spatially tailored mechanical behaviour via FFF.

The findings establish critical processing-structure-property relationships for FFF-fabricated zirconia lattice structures, providing evidence-based guidance for architectural selection in mechanically demanding applications such as bone implants. For compression-dominated applications, grid geometries offer maximum load-bearing capacity; for damage-tolerant designs, gyroid architectures provide enhanced deformation stability; and for multiaxial loading scenarios, triangular geometries deliver balanced performance.
Future work should extend this investigation to additional lattice topologies, evaluate fatigue and dynamic loading responses, and optimise processing parameters for each architecture to improve mechanical reliability further. The graded design approach demonstrated in this study offers opportunities for patient-specific biomedical implants with stiffness gradients that match those of natural bone, potentially addressing the stress-shielding limitations of current orthopaedic devices.

References

1. *Caiazzo, F., Alfieri, V., Campanelli, S. L., and Errico, V., "Additive manufacturing and mechanical testing of functionally-graded steel strut-based lattice structures," *Journal of Manufacturing Processes*, vol. 83, pp. 717–728, 2022.*

2. *Korkmaz, M. E., Gupta, M. K., Robak, G., Moj, K., Krolczyk, G. M., and Kuntoğlu, M., "Development of lattice structure with selective laser melting process: A state of the art on properties, future trends and challenges," *Journal of Manufacturing Processes*, vol. 81, pp. 1040–1063, 2022.*

3. *Wang, M., Zhang, J., Wang, W., and Gao, L., "Compression behaviors of the bio-inspired hierarchical lattice structure with improved mechanical properties and energy absorption capacity," *Journal of Materials Research and Technology*, vol. 17, pp. 2755–2771, 2022.*

4. *Traxel, K. D., Groden, C., Valladares, J., Bandyopadhyay, A., and Keck, W. M., "Mechanical properties of additively manufactured variable lattice structures of Ti6Al4V," *Materials Science and Engineering A*, vol. 809, p. 140925, 2021.*

5. *Wang, Y. J., Feng, C. X., Zhang, Z. J., Qian, D., and Song, Z. X., "Compressive property of additively-manufactured micro-*

*architectures with X-type lattice unit cell," *Materials*, vol. 15, p. 3815, 2022.*

6. *Park, M., Venter, M. P., and Plessis, A. D., "Simulation of the compression testing of additively manufactured lattice structures using inputs from microcomputed tomography," *Materials Design & Processing Communications*, 2023, Art. no. 8000727.*

7. *Wang, M., Zhang, J., and Wang, W., "Compression and deformation behaviors of hierarchical circular-cell lattice structure with enhanced mechanical properties and energy absorption capacity," *Aerospace*, vol. 9, p. 786, 2022.*

8. *Ma, X., Zhang, N., and Tian, X., "A novel hybrid lattice structure for improving compression mechanical properties," *Mechanics of Advanced Materials and Structures*, vol. 31, pp. 5805–5822, 2023.*

9. *Arshad, A. B., Nazir, A., and Jeng, J. Y., "The effect of fillets and crossbars on mechanical properties of lattice structures fabricated using additive manufacturing," *International Journal of Advanced Manufacturing Technology*, vol. 111, pp. 931–943, 2020.Park, K. M., Min, K. S., and Roh, Y. S., "Design optimization of lattice structures under compression: Study of unit cell types and cell arrangements," *Materials*, vol. 15, p. 97, 2021.*

10. *Xu, Y., Han, G., Huang, G., Li, T., Xia, J., and Guo, D., "Properties evaluations of topology optimized functionally graded lattice structures fabricated by selective laser melting," *Materials*, vol. 16, p. 1700, 2023.*

11. *Guo, S., Ma, Y., Liu, P., and Chen, Y., "Mechanical properties of lattice structures with a central cube: Experiments and simulations," *Materials*, vol. 17, p. 1329, 2024.*

12. *Wei, Y. P., Yang, H., Cheng, J. C., Gao, P., Shi, J., Lin, F., and Yu, B., "Compression behavior of 316L lattice structures produced by indirect additive manufacturing," *China Foundry*, vol. 20, pp. 83–88, 2023.*

13. *Teng, F., Sun, Y., Guo, S., Gao, B., and Yu, G., "Topological and mechanical properties of different lattice structures based on additive manufacturing," *Micromachines*, vol. 13, p. 1017, 2022.*

14. *Jin, M., Feng, Q., Fan, X., Luo, Z., Tang, Q., Song, J., Ma, S., Nie, Y., Jin, P., and Zhao, M., "Investigation on the mechanical properties of TPMS porous structures fabricated by laser powder bed fusion," *Journal of Manufacturing Processes*, vol. 76, pp. 559–574, 2022.*

15. *Tripathi, Y., Shukla, M., and Bhatt, A. D., "Idealization through interactive modeling and experimental assessment of 3D-printed gyroid for trabecular bone scaffold," *Proceedings of the Institution of Mechanical Engineers, Part H*, vol. 235, pp. 1025–1034, 2021.*

16. *Kladovasilakis, N., Tsongas, K., Kostavelis, I., Tzovaras, D., and Tzetzis, D., "Effective mechanical properties of additive manufactured triply periodic minimal surfaces: Experimental and finite element study," *International Journal of Advanced Manufacturing Technology*, vol. 121, pp. 7169–7189, 2022.*

17. *Liu, W., Sang, L., Zhang, Z., Ju, S., Wang, F., and Zhao, Y., "Compression and resilient behavior of graded triply periodic minimal surface structures with soft materials fabricated by fused filament fabrication," *Journal of Manufacturing Processes*, vol. 105, pp. 1–13, 2023.*

18. *Catchpole-Smith, S., Sélo, R. R. J., Davis, A. W., Ashcroft, I. A., Tuck, C. J., and Clare, A., "Thermal conductivity of TPMS lattice structures manufactured via laser powder bed fusion," *Additive Manufacturing*, vol. 30, p. 100846, 2019.*

19. *Kim, K., Kim, G. H., Kim, H. G., Kim, H. J., and Kim, N., "Customizing the mechanical properties of additively manufactured metallic meta grain structure with sheet-based gyroid architecture," *Scientific Reports*, vol. 12, p. 19897, 2022.*

20. *Yang, X., Gong, Y., Zhao, L., Zhang, J., and Hu, N., "Compressive mechanical properties of layer hybrid lattice structures fabricated by laser powder bed fusion technique," *Journal of Materials Research and Technology*, vol. 22, pp. 1800–1811, 2022.*

21. *Dave, H. K., Karumuri, R. T., Prajapati, A. R., and Rajpurohit, S. R., "Specific energy absorption during compression testing of ABS and FPU parts fabricated using LCD-SLA based 3D printer," *Rapid Prototyping Journal*, vol. 28, pp. 1530–1540, 2022.*

22. *Zhang, C., Li, T., Deng, Q., and Li, X., "Compression behavior of 3D printed polymer TPU cubic lattice structure," *Materials Research*, vol. 25, p. e20220060, 2022.*

23. *Mathiazhagan, N., Sivakumar, N. K., Palaniyappan, S., and Rahaman, M., "Influence of printing-based factors on the mechanical properties of hexagonal lattice-structured 3D printed novel walnut shell/polylactic acid composite," *Journal of Thermoplastic Composite Materials*, vol. 37, pp. 713–742, 2023.*

24. *Egan, P. F., Khatri, N. R., Parab, M. A., and Arefin, A. M. E., "Mechanics of 3D-printed polymer lattices with varied design and processing strategies," *Polymers*, vol. 14, p. 5515, 2022.*

25. *Castanon-Jano, L., Palomera-Obregon, P., Blanco-Fernandez, E., and Indacoechea-Vega, I., "Analysis of manufacturing and material parameters in 3D-printed polylactic acid (PLA) parts filled with glass powder: Mechanical, economic, and environmental assessment," *International Journal of Advanced Manufacturing Technology*, vol. 128, pp. 1965–1979, 2023.*

26. *Bruson, D., Galati, M., Calignano, F., and Iuliano, L., "Mechanical characterisation and simulation of the tensile behaviour of polymeric additively manufactured lattice structures," *Experimental Mechanics*, vol. 63, pp. 1117–1133, 2023.*

27. *Hassan, I. M., Enab, T. A., Fouda, N., and Eldesouky, I., "Design, fabrication, and evaluation of functionally graded triply periodic minimal surface structures fabricated by 3D printing," *Journal of the Brazilian Society of Mechanical Sciences and Engineering*, vol. 45, p. 66, 2023.*

28. *Kalossaka, L. M., Mohammed, A. A., Sena, G., Barter, L., and Myant, C., "3D printing nanocomposite hydrogels with lattice vascular networks using stereolithography," *Journal of Materials Research*, vol. 36, pp. 4249–4261, 2021.*

29. *Schittecatte, L., Geertsen, V., Bonamy, D., Nguyen, T., and Guenoun, P., "From resin formulation and process parameters to the final mechanical properties of 3D printed acrylate materials," *MRS Communications*, vol. 13, pp. 357–377, 2023.*

30. *Xiao, R., Ding, M., Wang, Y., Gao, L., Fan, R., and Lu, Y., "Stereolithography (SLA) 3D printing of carbon fiber-*

*graphene oxide reinforced polymer lattices," *Nanotechnology*, vol. 32, p. 235702, 2021.*

31. *Zeng, Y. S., Hsueh, M. H., and Hsiao, T. C., "Effect of ultraviolet post-curing, laser power, and layer thickness on the mechanical properties of acrylate used in stereolithography 3D printing," *Materials Research Express*, vol. 10, p. 025303, 2023.*

32. *Zhao, W., Wang, C., Xing, B., Shen, M., and Zhao, Z., "Mechanical properties of zirconia octet truss structures fabricated by DLP 3D printing," *Materials Research Express*, vol. 7, p. 085201, 2020.*

33. *Yang, J., Chen, X., Sun, Y., Zhang, J., Feng, C., Wang, Y., Wang, K., and Bai, L., "Compressive properties of bidirectionally graded lattice structures," *Materials & Design*, vol. 218, p. 110683, 2022.*

34. *Chen, W., Gu, D., Yang, J., Yang, Q., Chen, J., and Shen, X., "Compressive mechanical properties and shape memory effect of NiTi gradient lattice structures fabricated by laser powder bed fusion," *International Journal of Extreme Manufacturing*, vol. 4, p. 045002, 2022.*